Full length article

Experimental investigation of buckling and post-buckling behaviour of repaired composite laminates under in-plane shear loading

M. Damghani [*], A. Bugaje, G.A. Atkinson, D. Cole

School of Engineering, University of the West of England (UWE), Bristol, BS16 1QY, UK

ABSTRACT

The performance of Ramped Scarf (RS) and Stepped Scarf (SS) repair schemes for highly loaded composite structures has been extensively studied under compressive, tensile, and flexural loadings. However, there is a lack of research on the buckling and post-buckling behaviour of RS and SS repairs under in-plane shear loading, which is critical for aerostructures. This paper addresses this gap by investigating the buckling and post-buckling performance of these repair schemes. Pristine (P) laminates, RS repairs with a scarf angle of 3°, and SS repairs with an overlap step length of 1/60 were manufactured and tested. The quality of the scarf repairs was inspected using artificial intelligence-based machine vision. Mechanical in-plane shear testing was conducted to evaluate the buckling and post-buckling behaviour of P, RS, and SS laminates. The experimental results indicate that RS repairs demonstrated an average of 35 % higher maximum displacement and 12 % higher failure load compared to pristine laminates. SS repairs showed 19 % higher maximum displacement, and 5 % higher failure load compared to pristine laminates. RS repairs excelled in all key mechanical performance indicators, including buckling load, Hooke's stiffness, maximum displacement, and failure load, compared to SS repairs. The failure modes of P, RS, and SS laminates were similar. However, RS repairs exhibited greater susceptibility to repair patch detachment compared to SS repairs.

1. Introduction

There has been a significant rise in the use of composite laminates made of Carbon Fiber Reinforced Polymers (CFRP) in both civil and military aerostructures. These materials are predominantly used in the manufacture of primary and secondary structures of modern commercial aircraft. Primary structures are critical for structural integrity as they carry flight, pressurization, or ground loads, whereas secondary structures, if failed, would affect the operation of the aircraft but not lead to its loss. The extensive use of CFRP in these applications is attributed to their high specific stiffness (stiffness-to-weight ratio) and high specific strength (strength-to-weight ratio). Additionally, the mechanical properties of CFRP can be tailored by adjusting the fibre orientation, ply shape, and lay-up [1]. CFRP components also demonstrate enhanced performance under cyclic fatigue loading [2] and possess significantly improved corrosion resistance [3] compared to their metallic counterparts. Furthermore, fibre-reinforced parts are often designed integrally to reduce the overall number of parts, which is a considerable advantage over metallic structures.

Despite their advantages, CFRP laminates are susceptible to transverse impacts, which can result in Barely Visible Impact Damage (BVID) or Visible Impact Damage (VID) [4]. Sources of such impacts include:

- Tool drop during manufacture or regular inspection/maintenance,
- Debris impact during landing or taking off,
- Hail impact,
- Tyre burst impact during landing,
- Bird strike,
- Lightning strike,
- Collision with ground equipment.

Depending on the impact energy, these incidents can cause matrix cracking, delaminations, and fibre breakage. Particularly in severe cases involving fibre breakage, repairing the damaged part is essential to restore both the stiffness and strength of the structure.

Repair of CFRP laminates can be achieved through mechanical fastening [5], adhesive bonding [6], or a hybrid of the two [7]. Currently, the lack of non-destructive inspection techniques to detect

---

* Cortresponding author.
E-mail address: mahdi.damghani@uwe.ac.uk (M. Damghani).

weak bonds and unreliability of bonded joints in composites [8-10] complicates the certification of bonded repairs. As a result, bolted repairs are the current standard for primary load bearing aerostructures, as they ensure regulatory compliance. However, structural adhesive repairs are preferred for composite primary structures to achieve lighter, more aerodynamic configurations. This method is viable only when the damage after clean-up is not critical under in-service limit loads. This conservative, fail-safe requirement ensures that if the patch bond fails, the structure retains sufficient strength to complete the operation safely [11]. Current repair schemes, including stepped and ramped scarfs, aim to minimise stress within the adhesive, creating designs with shear-dominant stress states and minimal peel in the adhesive layer [12]. Hence, research has focused on the behaviour, stiffness, and strength performance of scarf repairs with shallow angles [13,14], primarily under tensile [15], compressive [16], or bending [17] loading. Certified repair schemes are thus constrained to a narrow set of joint designs. Recoverable static strength has been shown to range between 20 % and 83 % [18,19], with the latter achieved using a scarf angle of 2°. However, the requirement for small scarf angles is a significant limitation, as the repair patch must be considerably larger than the original damage area.

To optimize repair schemes and minimize the volume of undamaged material removed, research has focused on reducing repair size. Niedernhuber et al. [20] introduced fibre-oriented repair, significantly reducing repair size compared to conventional ramped, stepped, or scarf repair schemes. Similarly, Damghani et al. [18] developed the Variable Length Stepped Scarf (VLSS) repair scheme, which also reduced repair size and restored near-static strength of the structure. Most research has focused on the performance of repairs under tensile or compressive loading. For instance, Truong et al. [21] developed the Damage Zone Method (DZM), embedded in Finite Element Analysis (FEA), to predict the load-bearing capacity of repaired laminates under tensile loading, showing predictions within ±16 % of experimental results. Ghazali et al. [22,23] studied the performance of pristine, damaged, and ramped scarf repairs of sandwich laminates under compressive and flexural loading, reporting 85 % strength recovery in flexural tests for repaired laminates compared to pristine ones. Sun et al. [24] investigated the tensile performance of scarf joints bonded with different scarf angles, using experiments and FEA simulations with Triangular Cohesive Zone Model (TCZM) and User Defined Cohesive Zone Model (UCZM) to predict the failure of ductile adhesives. They also examined the influence of ply stacking sequence and adhesive mechanical properties on joint strength, finding good accuracy between experimental and predicted failure loads.

Most research has focused on the strength of repaired composite laminates, with less attention given to their buckling and stability. Campilho et al. [25] conducted experimental and numerical studies on the buckling behaviour of carbon–epoxy adhesively bonded scarf repairs under pure compression, with scarf angles from 2° to 45°. They found that buckling strength increased with decreasing scarf angle up to a certain point, after which compressive stiffness and buckling strength dropped significantly. They concluded that reducing the scarf angle offers no substantial strength benefit. In a subsequent study [26], they investigated the effect of overlap length and repair patch thickness on the compressive buckling load of single- and double-sided strap repairs, finding that the finite element method could effectively predict outcomes and reduce experimental costs when appropriate fracture simulation criteria were used. Turan [27] examined the buckling behaviour of adhesively patch-repaired composite plates, both experimentally and numerically. He observed that critical buckling loads were higher for single and double patch-repaired plates compared to plates without cutouts. He also noted that load eccentricity in single-patch repairs could negatively impact buckling load capacity. Deng et al. [28] used a numerical progressive damage model to predict buckling strengths and failure mechanisms in symmetric and asymmetric patch-repaired carbon-fibre reinforced laminates under compression without lateral restraints. They simulated patch debonding using a cohesive zone model with a trapezoidal traction-separation law for ductile adhesive, introducing geometric imperfection through first-order linear buckling configuration. Their simulation accurately matched experimental observations, revealing that lateral deformation reversed normal stress distribution, leading to patch debonding. Fiber failure and matrix cracking were primarily in 0° and 90° plies, with more severe damage near the compression side. Most repairs failed due to patch debonding, and some thin-patch assemblies collapsed due to laminate failure from high flexibility. Detailed reviews on composite bonded repair are provided in [8-10].

The present study provides a novel contribution to the field by addressing the largely unexplored topic of buckling and post-buckling behaviour of repaired composite laminates under in-plane shear loading conditions. Although prior research has extensively examined the buckling behaviour of pristine composite laminates [29,30], there is a significant gap in understanding the specific impact of repair techniques - such as Ramped Scarf (RS) and Stepped Scarf (SS) repairs - on in-plane shear buckling and post-buckling performance. This research uniquely addresses this gap by establishing baseline data for pristine CFRP composite laminates and systematically comparing the performance of RS and SS repaired laminates under in-plane shear stresses. The study employs an innovative approach, utilizing advanced machine vision techniques to evaluate the quality of scarf repairs. Additionally, it provides new insights into force-displacement and stress-strain relationships, as well as shear failure paths, thus enhancing the understanding of repaired composite structures in aero-structural applications subjected to significant in-plane shear loading. Such applications include wing ribs (subjected to pure in-plane shear stresses), spar webs (experiencing in-plane shear combined with uniaxial compressive-tensile bending stresses), and wing skins (undergoing in-plane shear combined with membrane biaxial compressive-tensile stresses).

To comprehensively address the shear buckling and post-buckling behaviour of repaired composite structures, the objectives of the current study are:

(i) To establish the baseline shear buckling and post-buckling behaviour of Pristine (P) CFRP composite laminates.
(ii) To determine the shear buckling and post-buckling behaviour of Ramped Scarf (RS) repaired CFRP composite laminates.
(iii) To assess the shear buckling and post-buckling behaviour of Stepped Scarf (SS) repaired CFRP composite laminates.

The remainder of this paper is organised as follows: Section 2 outlines the scope of the research. Section 3 discusses materials used, the manufacture of pristine and repaired laminates, quality assurance via machine learning inspection, and the mechanical testing procedures. Results and discussions of the mechanical testing are presented in Section 4. Finally, Sections 5 and 6 conclude the findings and proposes directions for future research.

2. Scope

The present study investigates the repair efficiency of laminates under in-plane shear loading at ambient room temperature (15℃−25℃) and relative humidity of 50 %−60 %. However, since the repair of composite laminates involves bonded repair via structural adhesive, the structural performance could be affected by environmental degradation, such as changes in temperature and ambient moisture during manufacture and testing. It is well documented in the literature that high temperatures and high moisture levels can lead to adhesive deterioration (adhesive swelling) in bonded joints, resulting in significant strength reduction. For further information on the environmental effects on the strength of adhesive joints, refer to [31]. Furthermore, it should be noted that the repair process implemented in this study was

conducted manually. This approach introduces potential variabilities due to human factors, as the process of applying a repair patch is highly delicate. Manual operations, such as cutting the plies into an exact circular shape and their precisely positioning at the centre of the laminate, are difficult to execute with zero tolerance. These variations in manual repair techniques could contribute to differences in the final properties of the repaired laminates.

Therefore, the results, discussions, and conclusions of this study are applicable only to the manufacturing methodology and testing environment of the specimens as outlined in Section 3. Additionally, due to the lack of standards for the experimentation of present study, in-house testing apparatus and specimen design were used, consistent with similar previous studies [1,32-34].

3. Methodology

This section first presents the mechanical properties of the materials used in this study (Section 3.1). Section 3.2 covers the design and manufacture of pristine, ramped scarf and stepped scarf repairs. The mechanical testing procedures and quality control of scarfed specimens are detailed in Sections 3.3 and 3.4, respectively.

3.1. Materials

The composite material used in this study was twill woven pre-impregnated carbon fibre (T800) with an areal weight of 200 g m^{-12}. The carbon pre-pregs consisted of 48.84 % fibre by volume. The epoxy matrix used was VTC401, which was cured at 120 °C for 45 min in a heated press. The mechanical properties of the cured CFRP plies were determined in-house and are provided in Table 1. The adhesive used for repairs was a structural epoxy adhesive, XA120 150 g film. This adhesive is easy to handle and is compatible with out-of-autoclave cured pre-pregs. It also exhibits minimal shrinkage and has a very low coefficient of thermal expansion, reducing the risk of post-cure cracking. The minimum and maximum cure temperatures for this adhesive are 80 °C and 120 °C, respectively. The mechanical properties of the adhesive are provided in Table 2.

3.2. Design and manufacture of pristine and repaired laminates

Twelve pristine laminates, each measuring 220 mm × 220 mm, were manufactured for this study. The laminates were hand-laid with a quasi-isotropic symmetric and balanced lay-up of $[\pm45_3/0_3]_s$. This configuration was chosen to ensure a balanced distribution of high load-carrying plies (0/90° plies) and low load carrying plies (±45°), facilitating an effective comparison of the repair schemes. While hard laminates (representative of wing skin) or soft laminates (representative of wing spar web) could alternatively be used, the methodology would remain unchanged. The laminates were cured in a heated press for 70 min at 120 °C under a pressure of 100 psi. After curing, the laminates were trimmed to a final size of 200 mm × 200 mm using band saw cutter. The geometry and lay-up of the pristine laminates are illustrated in Fig. 1a.

Table 1
Mechanical properties of woven CFRP (VTC401-C200T-T800–37 %RW-1250) fabric plies.

Mechanical properties	Units	VTC401-C200T-T800
$E_{11} = E_{22}$ (elastic modulus in 1 & 2 directions)	MPa	68287
G_{12} (shear modulus in plane 1–2)	MPa	4700
S_t (tensile strength)	MPa	755
S_c (compressive strength)	MPa	702
S_S (shear strength)	MPa	102
Strain to failure	N/A	0.01
ν_{12} (Poisson's ratio)	N/A	0.04
t_{ply} (cured ply thickness)	mm	0.20

Table 2
Mechanical properties of structural adhesive film XA120 [18].

Mechanical properties	Units	XA120
E (modulus of elasticity)	MPa	1644
G (shear modulus) *	MPa	610
S_t (tensile strength)	MPa	30
S_S (shear strength) **	MPa	18
ν_{12} (Poisson's ratio)	N/A	0.35

* Estimated from $G = E/2(1 + \vartheta_{12})$ based on [35].
** Approximated from $0.5S_t + \mu$ for brittle adhesives where μ (standard deviation) is taken as an average of data from [22,36,37,38].

Out of the twelve cured laminates, four were reserved for pristine testing and labelled as P1, P2, P3 and P4. Another four laminates were used to manufacture Ramped Scarf (RS) repair laminates, labelled as RS1, RS2, RS3 and RS4 (see Fig. 1b). The remaining four were used to manufacture Stepped Scarf (SS) repair laminates, labelled as SS1, SS2, SS3 and SS4 (see Fig. 1c).

In aerospace applications, the stepped scarf repair scheme aims to minimise the repair size, governed by the parameter $\beta = t/L$ (as shown in Fig. 1c), while ensuring near-complete restoration of both stiffness and static strength of the pristine laminate. Minimising the repair size is crucial to limit the removal of healthy material during the preparation for the repair patch. This is particularly important for repairs on primary structures, such as aircraft wings, where large repairs could interfere with stringers and ribs. However, choosing a β value that restores maximum static strength may necessitate larger repairs. This choice is based on the need to restore the original load path of the structure, allowing sufficient overlap length to transfer membrane stresses from the parent laminate to the repair patch and back to the parent laminate via shear stress diffusion in the overlap region. Current industrial practices use $\beta = 1/45$ (Airbus) and $\beta = 1/60$ (Boeing) for secondary structures, focusing on static strength restoration. These repairs can be excessively large, especially if the damage to the composite laminate is deep. In this study, a β value of 1/60 was chosen to ensure sufficient overlap length L. This specific choice not only provides sufficient overlap but also facilitates direct comparison with the ramped scarf repair, where a β value of 1/60 corresponds to a scarf angle (α) of 3° (as shown in Fig. 1b). Additionally, the chosen overlap length contributes to minimising variability in the results associated with the selection of adhesive type. This careful selection reduces the likelihood of repair patch detachment from the parent laminate during the loading process, as it helps to mitigate high peel and shear stresses within the adhesive (refer to Section 3.3). By ensuring that the overlap length is sufficient, the repair is expected to remain securely bonded to the parent laminate, even under the stresses encountered during loading, thereby enhancing the overall reliability of the repair.

To manufacture RS and SS laminates, the pristine laminates were prepared/scarfed in ramps and steps, respectively, as illustrated in Fig. 2. This process assumed a circular damage size $D = 20$ mm located 6 plies below the top surface which is typical for low velocity impact events [39].

The preparation involved ramped scarfing for RS laminates and stepped scarfing for SS laminates. Eight pristine laminate plates (four for RS and four for SS) were machined using a Computer Numerical Control (CNC) milling machine (a Bridgeport 600 vertical milling centre). A 10 mm, 4-flute tungsten end mill was utilised, with a feed rate of 100 mm/min and a spindle speed of 7500 rpm. The cutter paths for each sample profile were programmed using FeatureCAM computer-aided manufacturing software, resulting in an optimized path and a 0.2 mm depth of cut per pass until the desired scarfing profile was achieved.

For SS, the four step scarfed laminates were lightly sanded manually using 120 grit sanding mesh. After sanding, the bonding surfaces were washed with distilled water, dried, and cleaned using alcohol. The
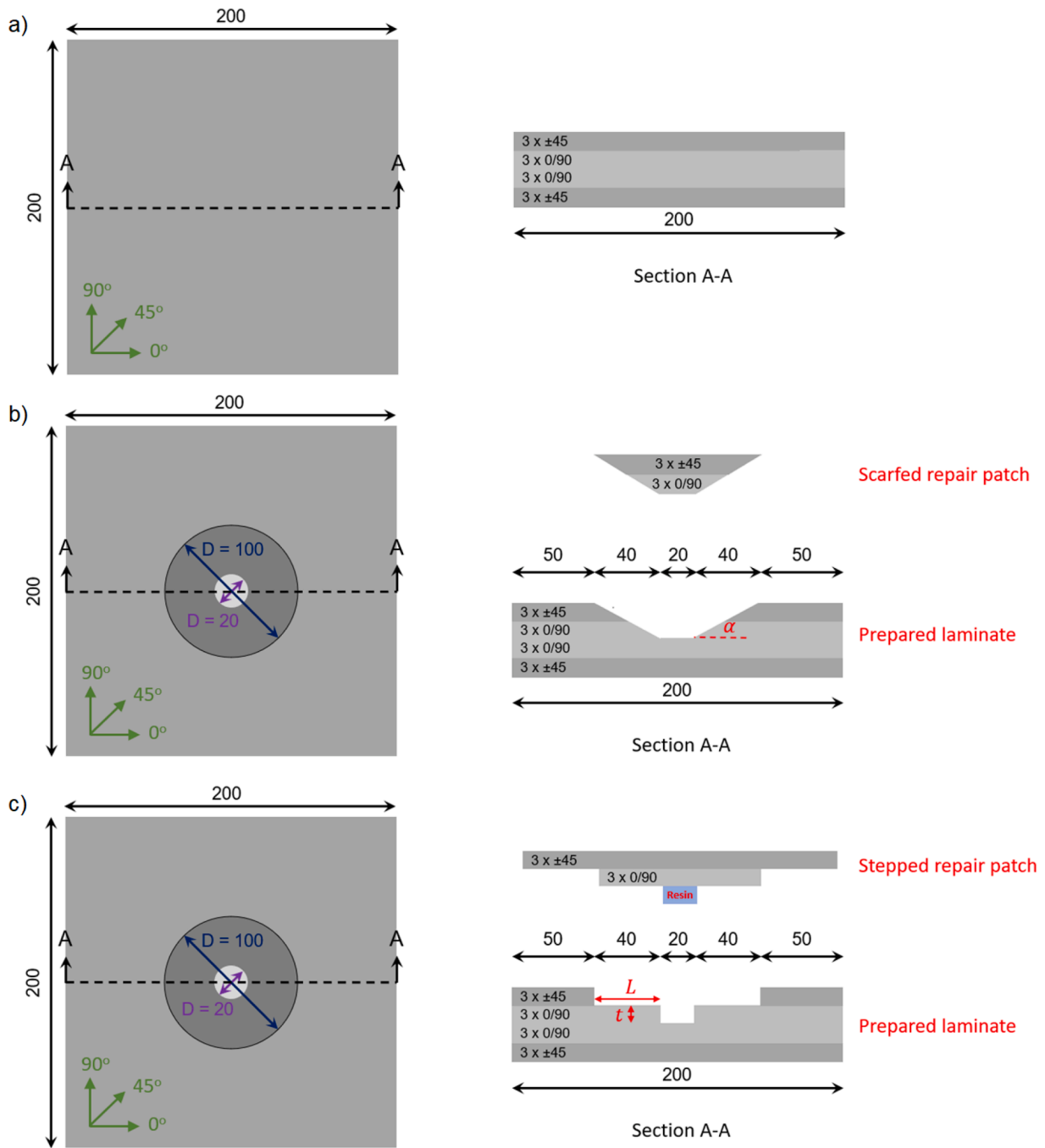
Fig. 1. Geometry and design of various repairs, a) pristine, b) ramped scarf (RS) and c) stepped scarf (SS) repairs (all dimensions are in ***mm***).

damage void was filled with resin, as shown in Fig. 1c. Then, XA120 adhesive film was cut to size and applied to the prepared surfaces (Fig. 3b). The repair plies were cut to size and placed sequentially in position (Fig. 3c and Fig. 3d). To maintain constant bond thickness, 0.05 gs of chopped glass fibres were scattered through the adhesive, without having significant impact on the mechanical properties of the adhesive. The repaired laminates were then placed in a vacuum bag (Fig. 3e) and cured in oven at 120 °C (the curing temperature of the adhesive film) for 1 hour, followed by an additional 1 hour for post-cure (Fig. 3f).

For the manufacture of RS laminates, a similar procedure to that of SS laminates was followed. The sequence of repair activities for RS samples is illustrated in Fig. 4.

3.3. Shear buckling and post-buckling testing

The shear test was conducted using a 100 kN capacity INSTRON tensile machine equipped with a picture frame test fixture. The specimens were first clamped into the test fixture via grip plates of 10 mm width, resulting in gauge dimensions of 180 mm × 180 mm. The specimens were held in position and loaded by constant static friction via the clamping force of the bolts. The specimens, along with in-house manufactured test fixture, were then positioned in the tensile test machine (see Fig. 5). A tensile load was applied under displacement control at a speed of 2 mm/min, inducing shear deformation in the test laminate.

Shear buckling and post-buckling tests were conducted on the following test specimens:
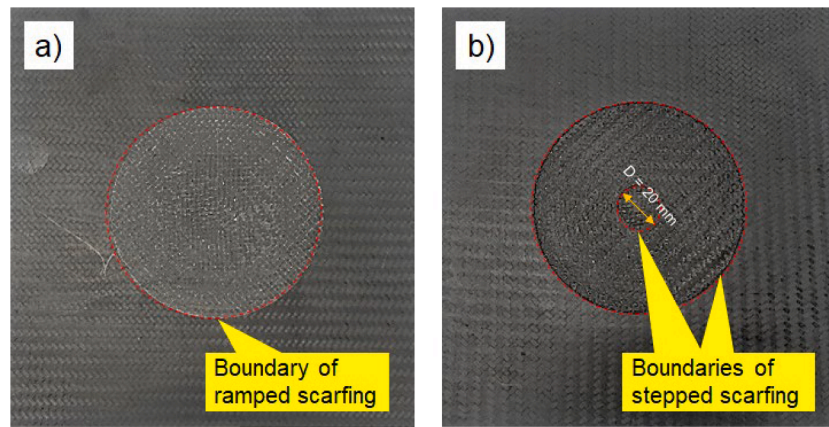
Fig. 2. Prepared laminates, a) ramped scarf, b) stepped scarf.
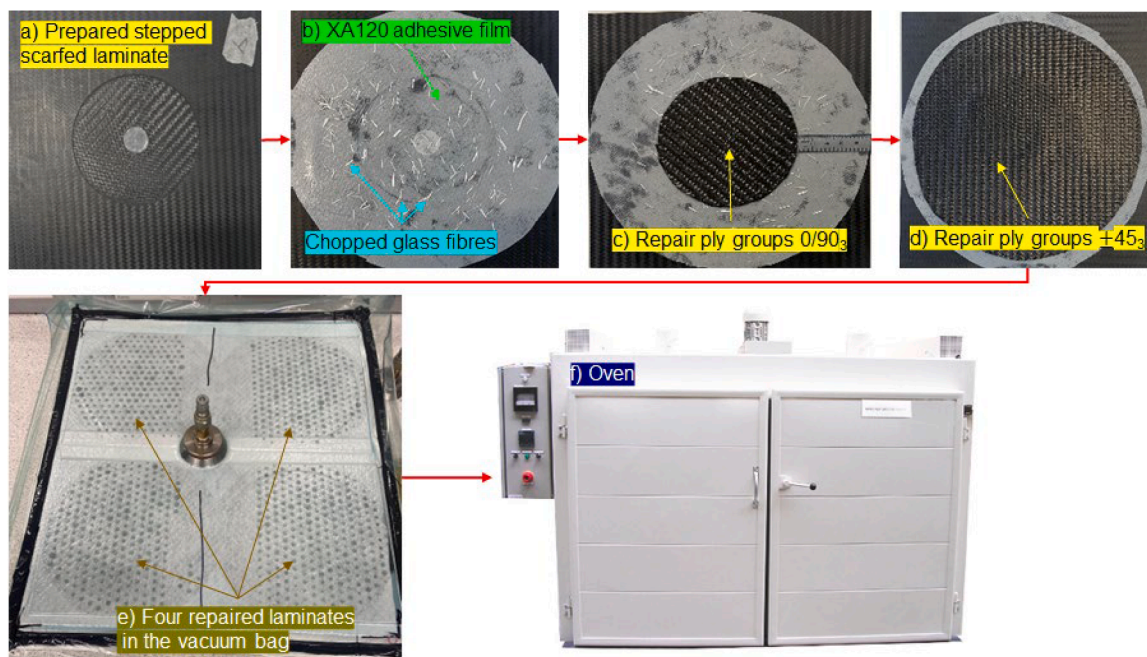

Fig. 3. Sequence of repair process for stepped scarf repair.

- Four Pristine (P) samples,
- Four Ramped Scarf (RS) repaired samples,
- Four Stepped Scarf (SS) repaired samples.

This resulted in a total of twelve test cases. Throughout the tests, average strains along the loading direction within the repaired portions of the specimens were measured. These strains were obtained using an INSTRON AVE2 Non-contacting Video Extensometer, which measures the movement of two white dots positioned a certain distance apart in the middle of the specimens (see Fig. 5). This strain measurement technique allowed continuous monitoring up to the point of failure without pausing the test, providing more accurate and representative results. Additionally, one specimen from each test group (P, RS, and SS) was strain gauged using strain gauges with a grid resistance of 120.0 ± 0.3 % Ω. This was done to monitor the flow of strains from the parent laminate to the repair patch and back to the parent laminate. The size of the strain gauges was larger than the carbon fibre pitch in both weft and warp directions to allow accurate average strain readings on the woven laminate. The locations of the strain gauges for each test group are shown in Fig. 6. For all laminates, Strain Gauge 1 (SG1) was placed at the

centre on the front face of the laminates to provide strain readings perpendicular to the loading direction. Strain Gauge 2 (SG2) was placed at the same location and direction as SG1 but on the back face of the laminates to capture the bending moment effect after buckling at the central location. Central strains in the loading direction were already captured using the non-contact AVE2 method, so only two strain gauges were used for P laminates. For RS repairs, an additional strain gauge (SG3) was placed at the edge of the repair patch (Fig. 6b) to measure strains in the loading direction. For SS repaired laminates, Strain Gauges 3 (SG3) and 4 (SG4) were placed just before the repair ply group overlaps, both reading strains in the loading direction (Fig. 6c). This setup ensured the monitoring of strain flow and potential detachment of the repair patch during the test.

3.4. Machine vision verification of steeped and ramped scarfs

As in previous work [18], a machine vision method was used to verify the quality of the scarf repairs. This method involves capturing a "polarisation image" of the specimen, which indicates both the intensity and angle of polarization of incoming light. The advantage of a

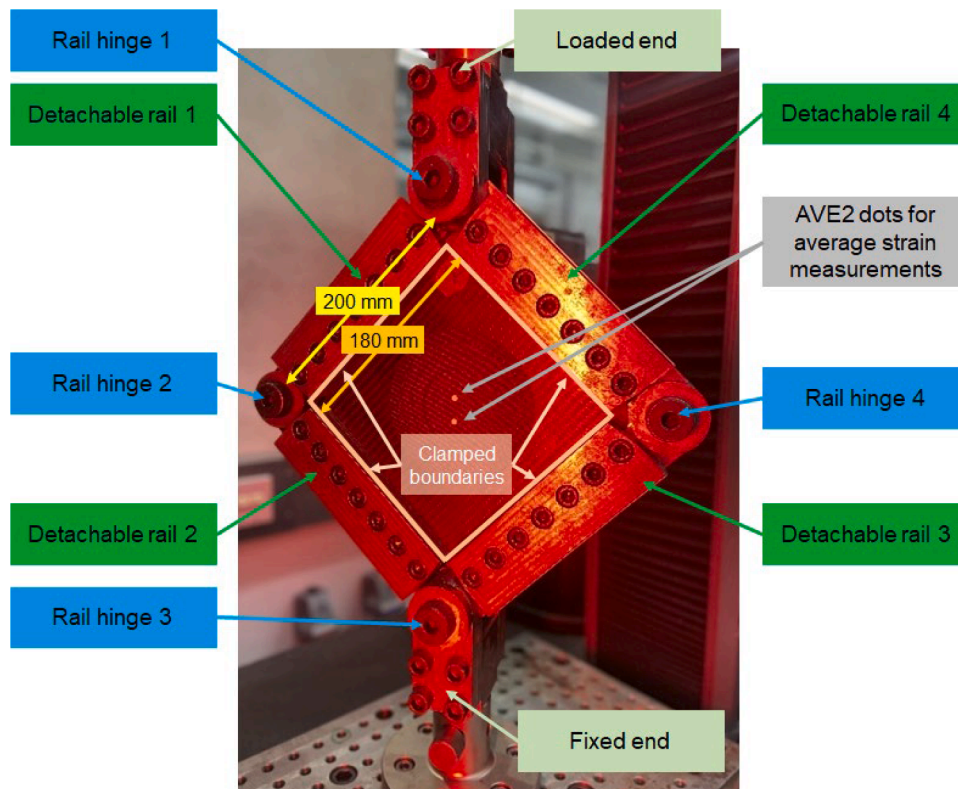**Fig. 4.** Sequence of repair process for ramped scarf repair.

Fig. 5. In-plane shear test set-up.

polarisation image is that the anisotropically conducting fibres near the surface of the sample cause reflected light to become polarised in a plane defined by the fibre orientation at each pixel and the optical axis of the camera. This enables the generation of an image where each pixel angle encodes an estimate of the fibre direction, allowing for a detailed

assessment of the scarf quality.

Fig. 7 presents a polarisation image of a stepped scarf. The image clearly shows $\pm 45°$ fibres outside the scarf and successful material removal down to the $0/90°$ layer in the centre. The intermediate regions display a mixture of each layer, indicating that the machining process
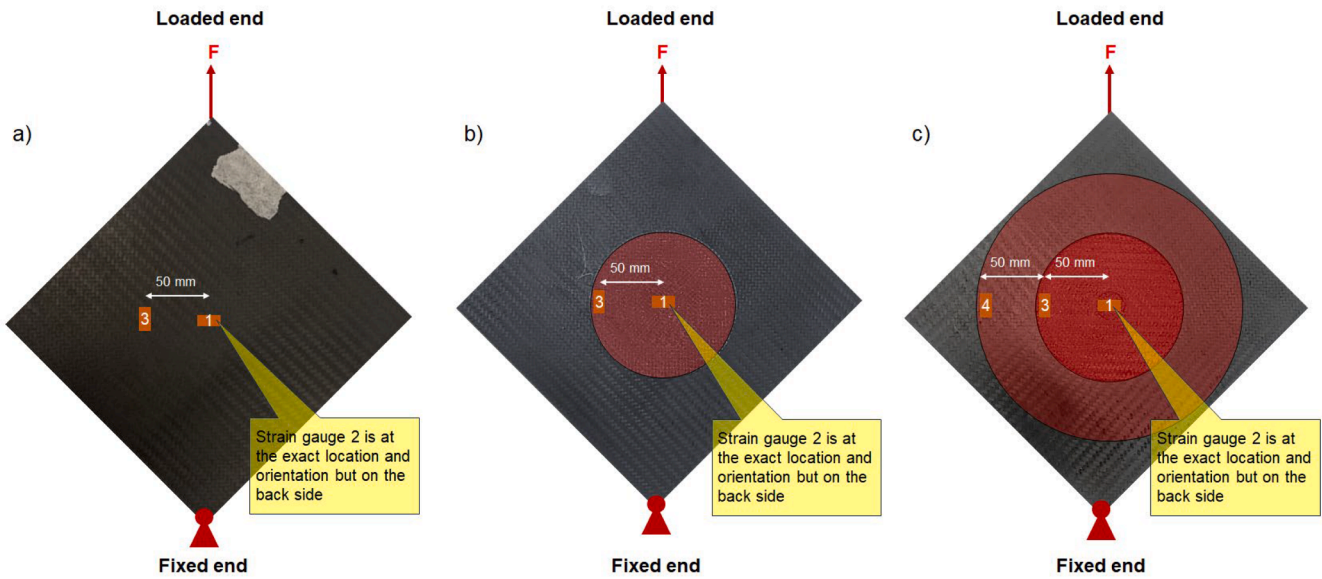
Fig. 6. Strain gauges positioning for, a) pristine (P), b) RS and c) SS repairs (in all cases, strain gauge 2 is at exact same location as strain gauge 1 but placed on the back face of the laminates).
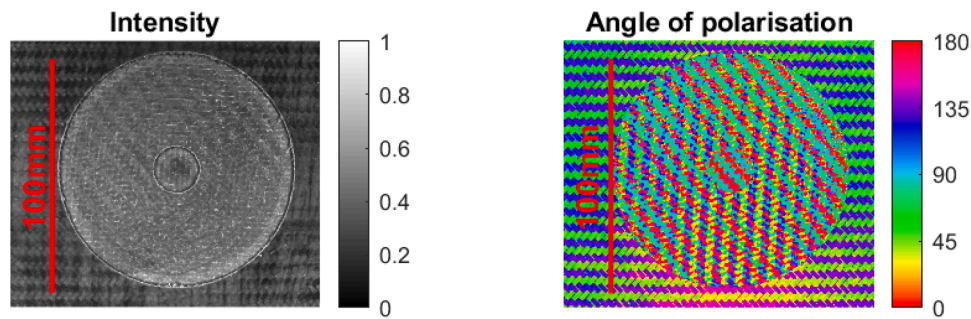
Fig. 7. Polarisation image for a stepped scarf.

was successful in reaching the required interface. A comparable example for the ramped scarf is shown in Fig. 8. For this study, all specimens were qualitatively assessed to be adequately machined within the possible tolerances of the adopted manufacturing method.

4. Results and discussions

In this section, the behaviours of pristine (P) and repaired specimens (RS and SS) are investigated. These effects are studied in terms of load-displacement response (Section 4.1), stress-strain behaviour (Section 4.2), and visual assessment of the failure modes (Section 4.3).

4.1. Load-displacement response

Fig. 9 illustrates typical instability behaviour of structures. Generally, the load-displacement of structures follows a linear primary path. However, upon reaching the buckling load (bifurcation point at F_{cr}), the structure can follow one of two possible secondary paths:

- **Secondary Post-Buckling Collapse Path:** In this scenario, the slope of the load-displacement graph becomes negative, indicating negative stiffness, which leads to the collapse of the structure.
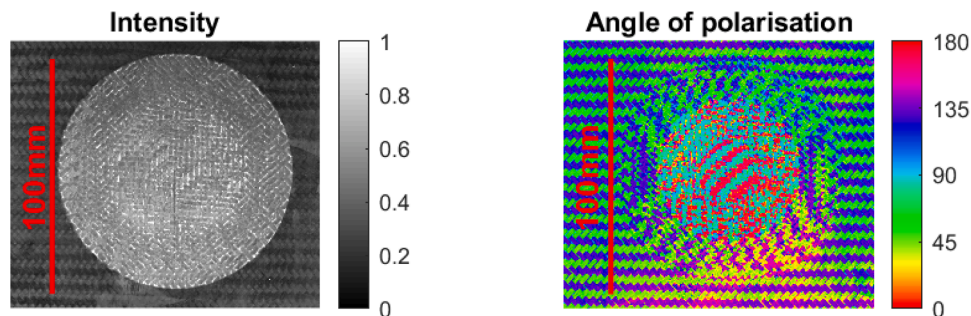
Fig. 8. Polarisation image for a ramped scarf.
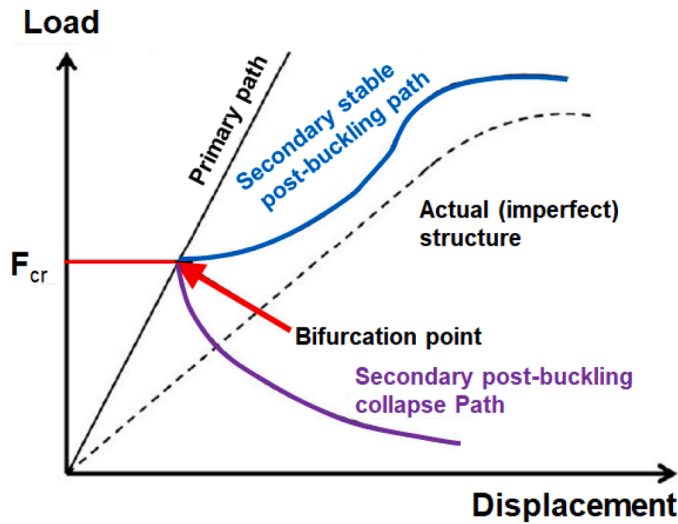
Fig. 9. Typical bucking and post-buckling behaviour of structures.

- **Secondary Stable Post-Buckling Path:** Here, the structure continues to endure higher loads as displacement increases, exhibiting positive stiffness and stable behaviour.

For a perfect structure, the transition between the primary and secondary paths is discernible as a clear bifurcation point. However, in the case of an imperfect structure, there is a smooth transition between the primary and secondary paths [1,32,34].

In the present study, during mechanical testing, the displacement of the loaded end (see Fig. 6) was recorded against the applied load. The load-displacement behaviours of pristine, RS and SS repairs are presented in Fig. 11. Key Mechanical Performance Indicators (MKPI), including buckling load, maximum displacement, failure load and Hooke's stiffness are summarised in Table 3 and illustrated graphically in Figs. 12-14.

Table 3
Key mechanical performance indicators of pristine, RS and SS repaired laminates.

Specimen ID	Buckling Load (kN)	Maximum Displacement (mm)	Maximum Load (kN)	Hooke's Stiffness (kN/mm)
P1 [I]	26.11	18.36	67.83	21.60
P2	25.22	15.86	66.70	24.10
P3	22.10	14.27	58.63	23.79
P4	21.99	18.89	58.11	23.99
Average	23.86	16.84	62.82	23.37
SD	2.12	2.17	5.16	1.19
Average ± SD	23.86 ± 2.12	16.84 ± 2.17	62.82 ± 5.16	23.37 ± 1.19
RS1 [II]	28.61	21.77	66.27	24.46
RS2	21.01	N/A [IV]	N/A [IV]	24.35
RS3	22.33	26.09	72.15	24.53
RS4	27.73	20.30	73.26	25.68
Average	24.92	22.72	70.56	24.75
SD	3.81	3.01	3.76	0.62
Average ± SD	24.92 ± 3.81	22.72 ± 3.01	70.56 ± 3.76	24.75 ± 0.62
SS1 [III]	17.95	22.80	79.00	19.96
SS2	19.36	21.15	65.78	20.55
SS3	16.98	15.57	49.87	19.52
SS4	25.71	20.83	70.30	21.77
Average	20.00	20.09	66.24	20.45
SD	3.93	3.14	12.21	0.98
Average ± SD	20 ± 3.93	20.09 ± 3.14	66.24 ± 12.21	20.45 ± 0.98

I Pristine.
II RS is Ramped Scarf repair.
III SS is Stepped Scarf repair.
IV Specimen failed prematurely after linear portion of load-displacement graph.

Based on Fig. 11, the pristine (P), Ramped Scarf (RS), and Stepped Scarf (SS) repairs exhibit a linear load-displacement behaviour up to displacements of approximately 1.5 mm to 1.7 mm, where buckling occurs. Fig. 12 presents the average buckling loads for the test specimens, with pertinent Standard Deviations (SD) represented as error bars. RS repairs demonstrate the highest average buckling load, indicating superior buckling performance compared to pristine and SS repair. However, it is important to consider the variability captured by the SDs. The overlap of the error bars indicates that the range of buckling loads for the RS and pristine samples might significantly overlap, suggesting that their buckling performance could be statistically similar. This implies that the apparent superiority of RS repairs, as inferred from the average buckling load values, might not be as pronounced when accounting for the variability in the data. Therefore, while RS repairs may show a trend towards higher buckling loads, the standard deviations suggest caution in definitively concluding that their performance is significantly better than that of pristine samples. Conversely, SS repairs perform poorly compared to pristine laminates in terms of buckling load. The observed reduction in performance can be attributed to load eccentricities present in Stepped Scarf (SS) repairs, where the overlapping repair plies are misaligned relative to their corresponding parent plies through the laminate thickness. Specifically, as shown in Fig. 10, an offset e exists between the mid-plane of the unrepaired section of the laminate and that of the repaired section. Consequently, the application of a shear force S brings about bending moment of $S.e$. These load eccentricities function as imperfections within the laminate, promoting premature buckling under shear loading conditions. SS repairs generally exhibit a less discernible transition between primary and secondary load path (see Fig. 11c). This is particularly evident in specimen 4, where the laminate behaves similarly to an imperfect structure, with a less distinct transition between primary and secondary load paths (see Fig. 9). It should be mentioned that, in such cases, the buckling load of an imperfect structure is generally expected to be lower than that of a perfect one. However, this is not observed with specimen 4, where the buckling load is unexpectedly higher. This discrepancy could be attributed to variability in the manufacturing of the repair specimens, particularly concerning the cured ply thickness of the repair patch, which directly affects the bending stiffness of the repaired laminate. Variations in the thickness of the cured plies may have led to increased bending stiffness, thereby influencing the buckling performance observed in specimen 4. A comparison of SDs suggests that repaired specimens, particularly SS repairs, show higher deviations from average values. This outcome is expected within the scope of the current study, as bonded repairs inherit vulnerabilities associated with bonded joints. The greater the number and length of bonded joints, the higher the vulnerabilities and data scatter, as observed in SS specimens. It is well established in the literature [40] that bonded joints are susceptible to various parameters, including variations in the manufacturing bonding process, geometric parameters (bond line thickness, joint configuration, overlap length), material parameters (adhesive properties, adherend material), and environmental factors (pre-bond moisture, post-bond moisture, temperature, combined moisture, and temperature). These factors lead to less reliable joints, often resulting in higher SDs, as demonstrated in earlier work by the authors [41].

As shown in Fig. 11, after reaching the buckling load (point of bifurcation), all laminates follow a stable secondary path, i.e. the post-buckling path. The behaviour of pristine and RS repair laminates resembles that of a perfect system, while the SS repairs, particularly specimen 4, exhibit behaviour more characteristic of an imperfect system.

Hooke's stiffness is defined as the slope of linear portion of the load-displacement response shown in Fig. 11. As depicted in Fig. 13, the stiffness of RS and pristine laminates are similar, with RS laminates showing a slightly higher stiffness, though this difference is negligible considering the standard deviation (SD). In contrast, SS repairs exhibit the least stiffness. This reduced stiffness is attributed to the offset
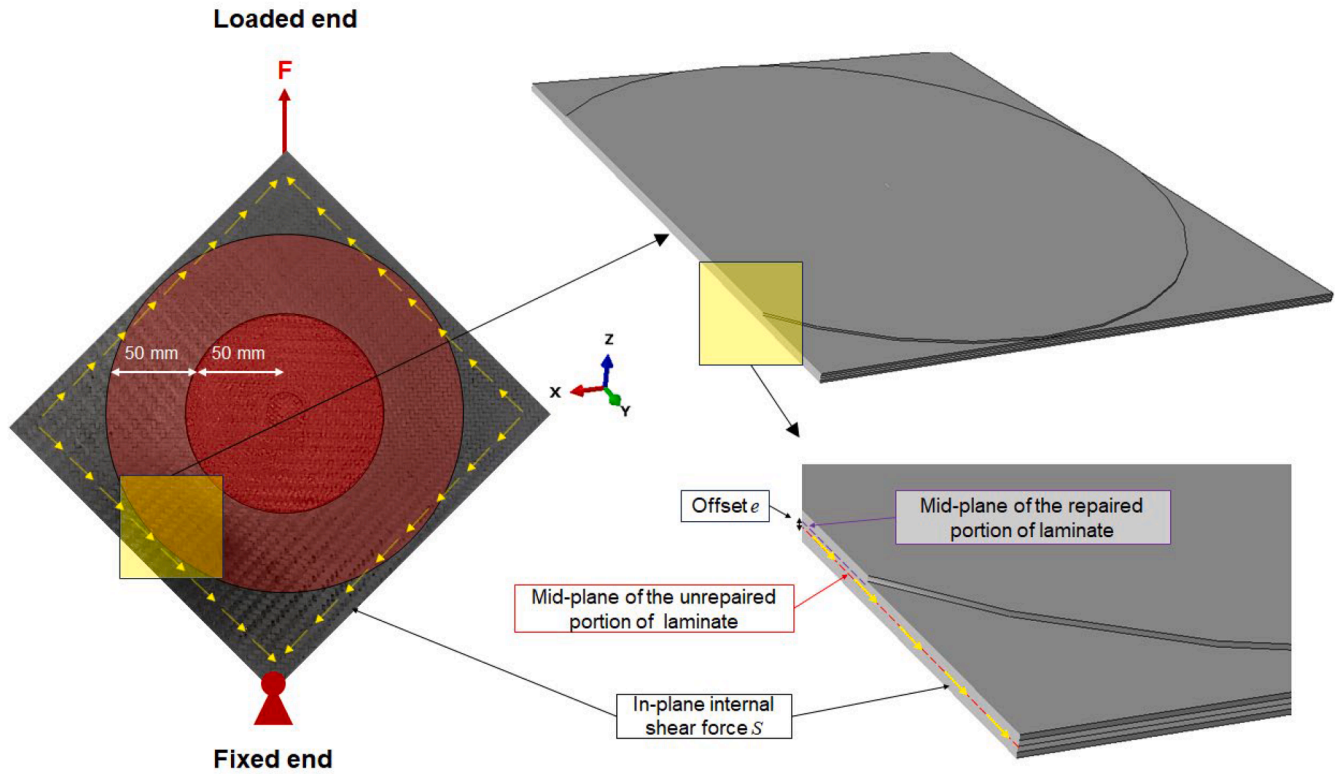
Fig. 10. Schematic illustration of load eccentricity in SS specimens.

between the parent and overlapping repair plies, resulting in load eccentricity.

Figs. 14 and Fig. 15 provide a comparison of maximum displacements and failure loads for all test specimens, respectively. It is evident that both repair types exhibit superior performance compared to pristine laminates. For instance, RS repairs demonstrate an average of 35 % higher maximum displacement and 12 % higher failure load than the pristine laminates. Similarly, SS repairs show 19 % higher maximum displacement, and 5 % higher failure load compared to the pristine laminates. As detailed in Section 4.2, the stepwise addition of material at varying depths in SS repairs leads to an increase in effective thickness, which in turn enhances the bending stiffness compared to pristine laminates. This increased stiffness improves the failure load capacity of the laminate. However, due to load eccentricity, the improvement in failure load observed with SS repairs does not reach the level achieved by RS repairs.

4.2. Stress-strain response

Shear stress and strain responses of P, RS and SS specimens are provided in Figs. 16-18. In these graphs, shear stress is analytically calculated as

$$\tau = \left(F \big/ \sqrt{2}\right) \big/ (w \times t) \tag{1}$$

where *F*, *w* and *t* are applied force, width of specimen (180 mm) and laminate thickness ($12 \times 0.22 = 2.64$ mm), respectively.

Based on Figs. 16-Fig. 18, stress-strain responses of P, RS and SS laminates respectively, show similar qualitative behaviour, characterised by three distinct regions:

- **Region 1 (Linear):** All laminates exhibit linear behaviour up to the green point, with no out-of-plane displacement. During this phase,

the laminates experience in-plane membrane stresses and deformations.
- **Region 2 (Post-Buckling and Nonlinear):** For P and RS laminates, the stress-strain behaviour from the green to the purple point indicates slight bending about the main diagonal direction (yellow dashed line). Despite this bending, strain gauges SG1 and SG2, placed at the centre but on opposite sides of the specimens, show compressive stresses.
- **Region 3 (Post-Buckling and Nonlinear):** As the load increases from the purple to the red point, the bending curvature of P and RS laminates increases. This increased curvature leads to a reversal of the strains recorded by SG1 from negative (compressive) to positive (tensile).

It is important to note that for SS laminates, the behaviour in regions 2 and 3 differs from that of P and RS laminates. This difference arises from the inherent load eccentricities and imperfections in SS repairs, which affect their post-buckling performance and overall stability. This phenomenon is detailed in the previous work of Damghani et al. [1]. The SS laminates show a less consistent and more variable stress-strain response in these regions compared to P and RS laminates.

To explain the quantitative differences between the stress-strain behaviour of P and RS laminates compared to SS, it is important to compare their analytical bending stiffnesses (d_x and d_y). These bending stiffnesses are defined as follows:

$$d_x = E_x I = \frac{12 \times E_x}{t^3} \tag{2}$$

$$d_y = E_y I = \frac{12 \times E_y}{t^3} \tag{3}$$

where E_x, E_y, I, t are homogenised modulus in the loading direction (x), perpendicular to the loading direction (y), second moment of area and laminate thickness, respectively. d_x, d_y are bending stiffnesses about x
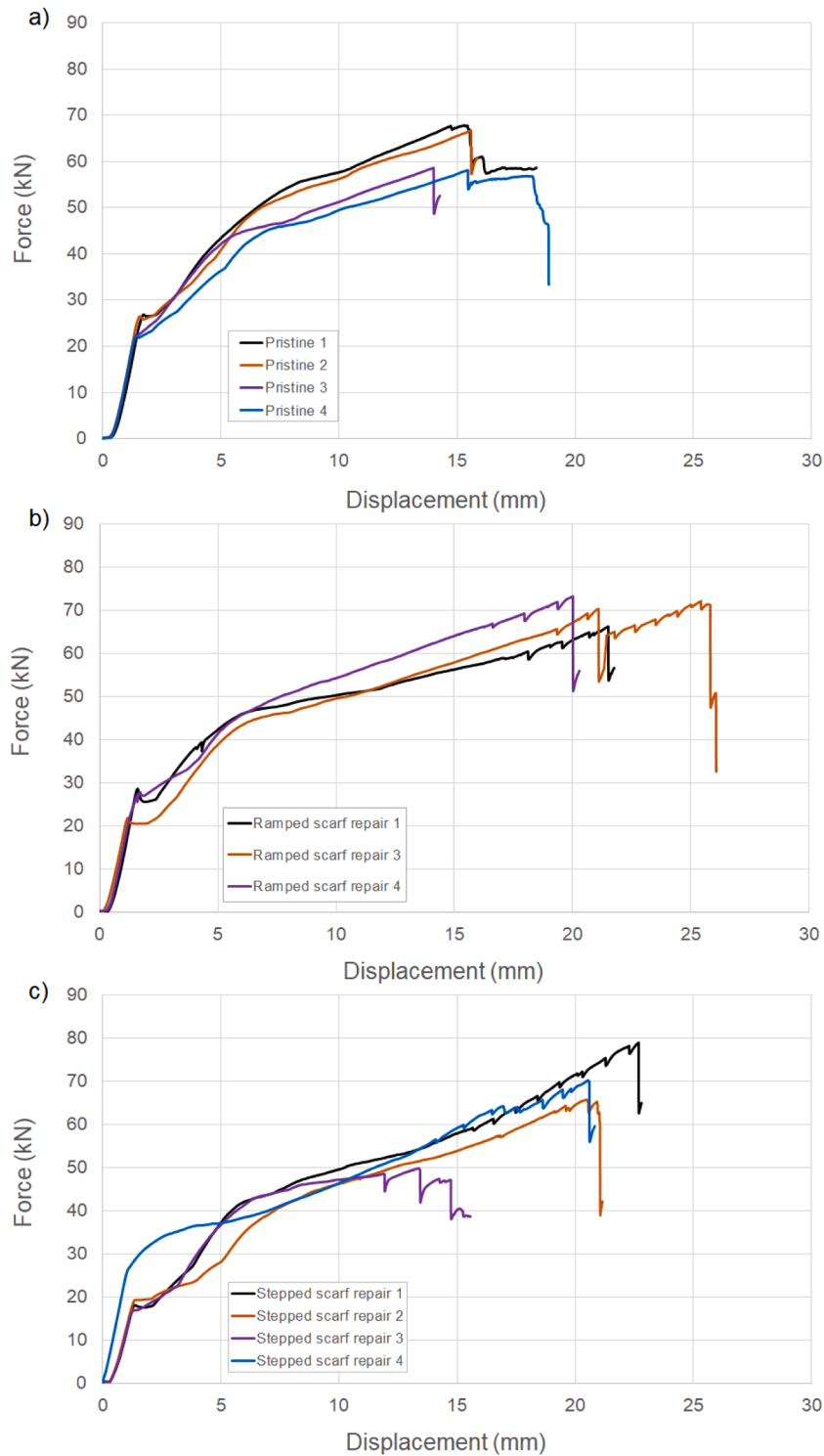
Fig. 11. Load-displacement behaviour of test specimens, a) Pristine, b) Ramped Scarf (RS) repair and c) Stepped Scarf (SS) repair (Note: specimen RS2 failed prematurely after linear portion of load-displacement graph which prevented a complete post-buckling response from being recorded).

and y axes, respectively. The bending stiffnesses over the domain of each laminate are illustrated in Fig. 19. The similarity in the stress-strain response behaviour of P and RS laminates is attributed to their consistent bending stiffness across the entire laminates, as shown in Fig. 19a-b. In contrast, the distribution of bending stiffness in the SS repair laminate is more complex, with varying values across different zones as below (see Fig. 19c):

- **Zone A:** This is where the resin pocket fills the removed damage. In this zone, the bending stiffness is approximately 6 % higher than that of the parent structure.
- **Zone B:** This zone corresponds to the repair overlap plies of $[0/90]_3$. The bending stiffness in this zone is approximately 24 % higher than that of the parent laminate.
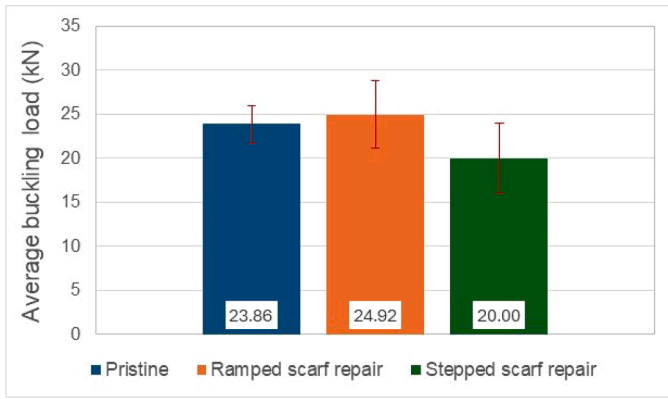
Fig. 12. Comparison of average buckling load.

- **Zone C:** This zone corresponds to the repair overlap plies of $[\pm 45]_3$. The bending stiffness here is approximately 13 % lower than that of the parent laminate.

The significantly higher bending stiffness in zones A and B (especially the 24 % increase in zone B) results in a stiffer laminate, which undergoes less out-of-plane deflection in the post-buckling regions 2 and 3. Consequently, although SG1 and SG2 show a similar qualitative response, they present significantly less strain in SS laminates compared to P and RS laminates. This variability in bending stiffness explains the quantitative differences observed in the stress-strain behaviours of these laminates.

Finally, at the end of the test (red point), the laminates begin to fracture mostly symmetrically for both P and RS specimens, as indicated by the blue dotted lines in Figs. 16 and Fig. 17. Notably, for RS specimens, the ramped repair patch detaches precisely at the point of failure (red point), demonstrating an excellent bond with the parent laminate. Throughout the test, the average strain readings from the INSTRON AVE2 Non-contacting Video Extensometer consistently show tensile strains in the loading direction, in agreement with the findings of [32]. Full details of failure modes are provided in Section 4.3.

4.3. Failure modes

The failure mode of each test specimen is provided in Tables 4-6 for P, RS and SS laminates, respectively.

As summarised in Table 4, for the P specimens, the predominant failure mode is characterized by fibre breakage along the main diagonal of the specimens, initiated on the compressive side (i.e., the back face of the laminates). This outcome is anticipated, as the compressive strength of the material is lower than its tensile strength, as indicated in Table 1. As a result, during bending about the main diagonal axis, the fibres on the back face are subjected to compressive stresses and are the first to fail. This is subsequently followed by fibre breakage on the tension side,
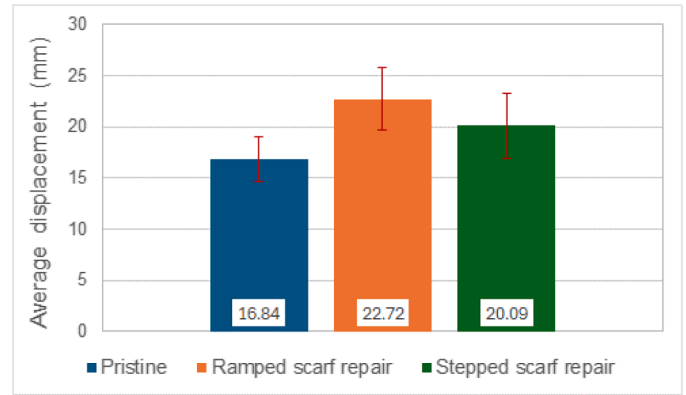
Fig. 14. Comparison of average values maximum displacement.
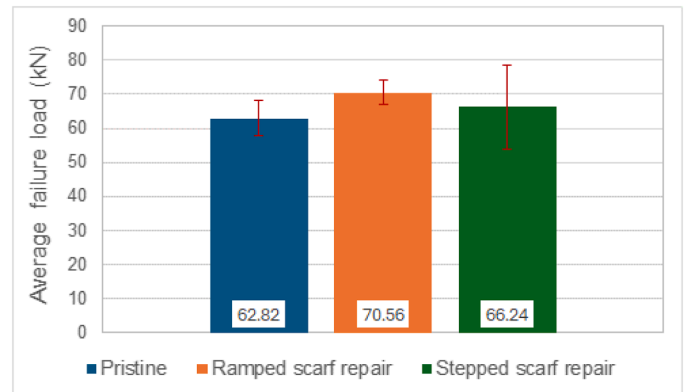
Fig. 15. Comparison of average failure load.
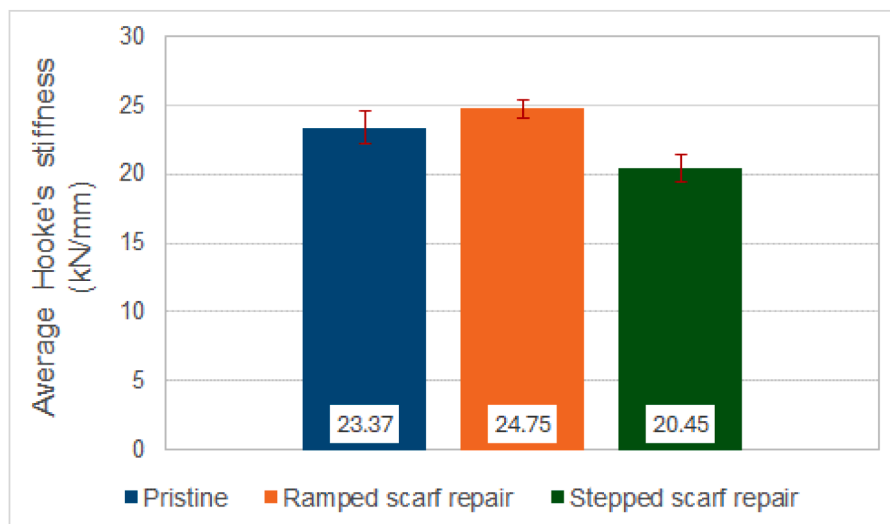
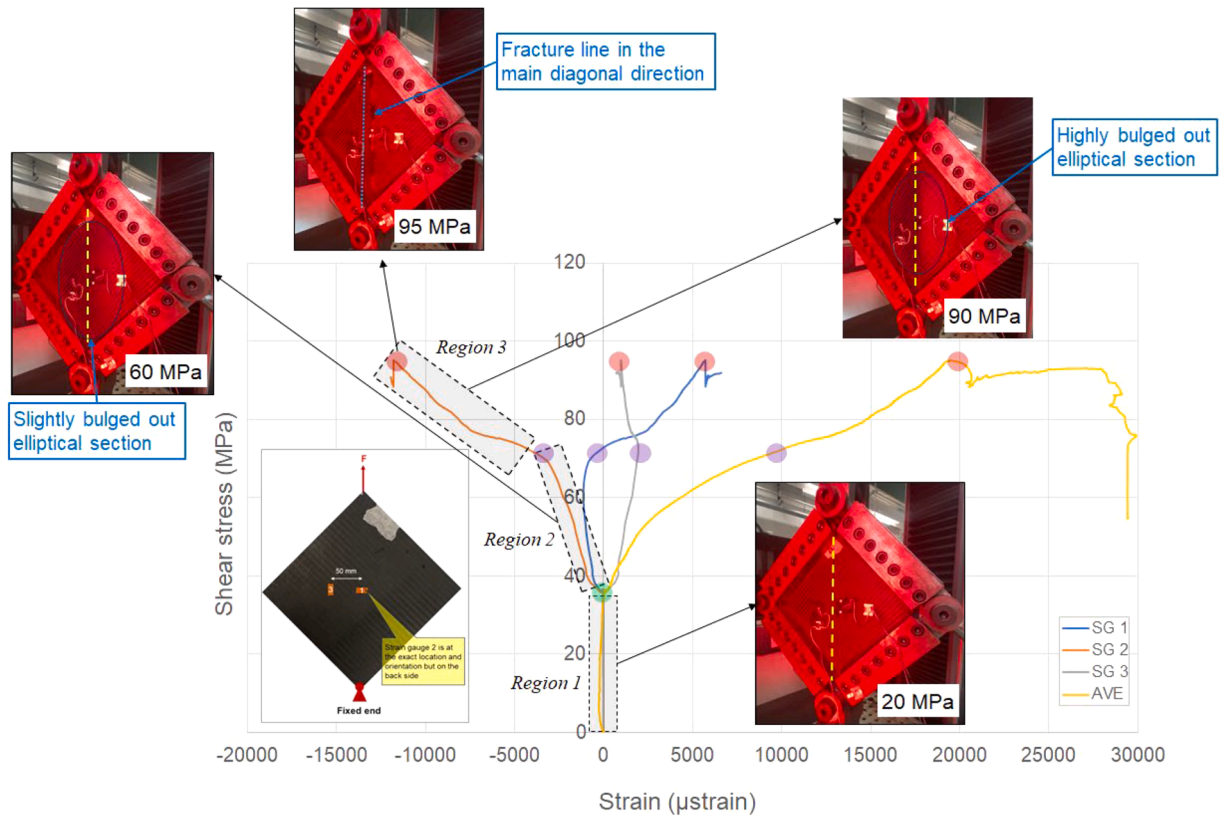**Fig. 13.** Comparison of average Hooke's stiffness.
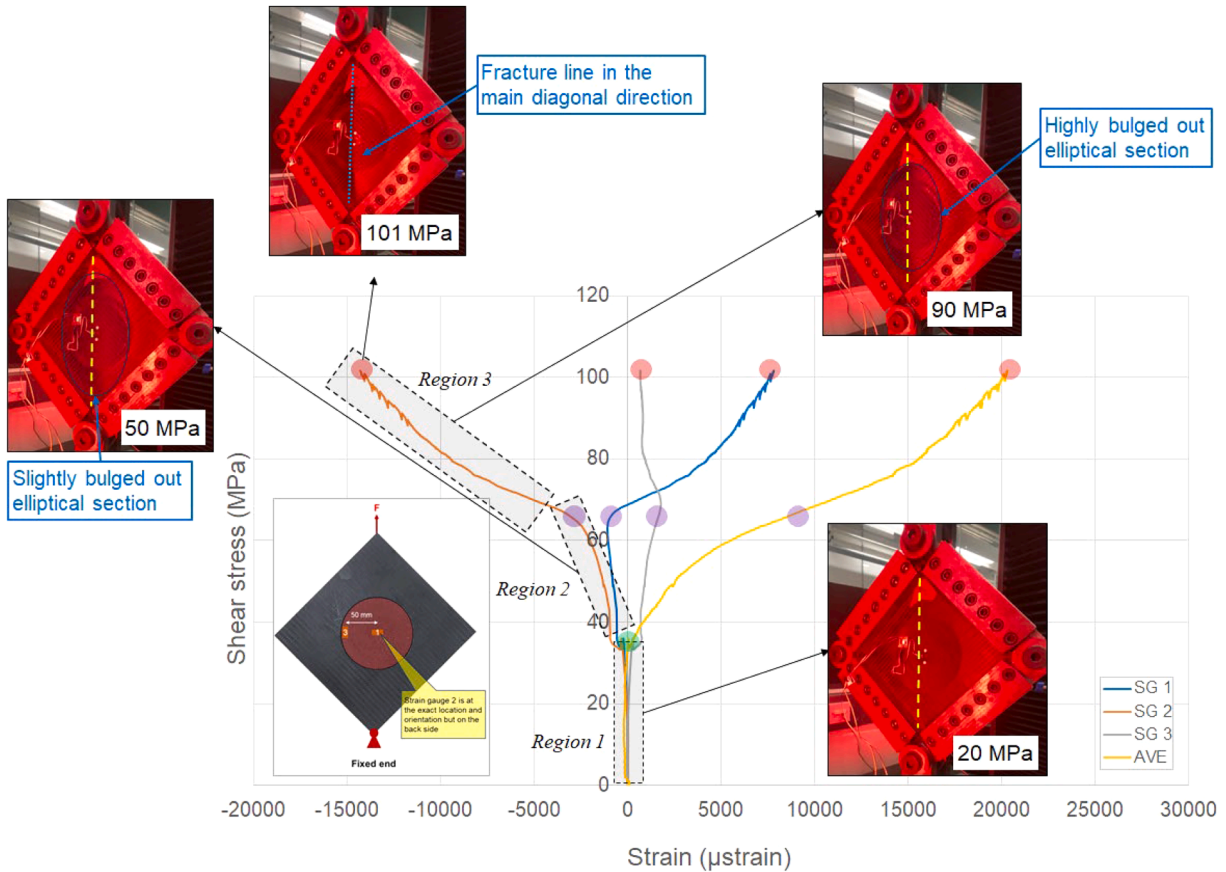
Fig. 16. Shear stress vs. strain of pristine laminates.
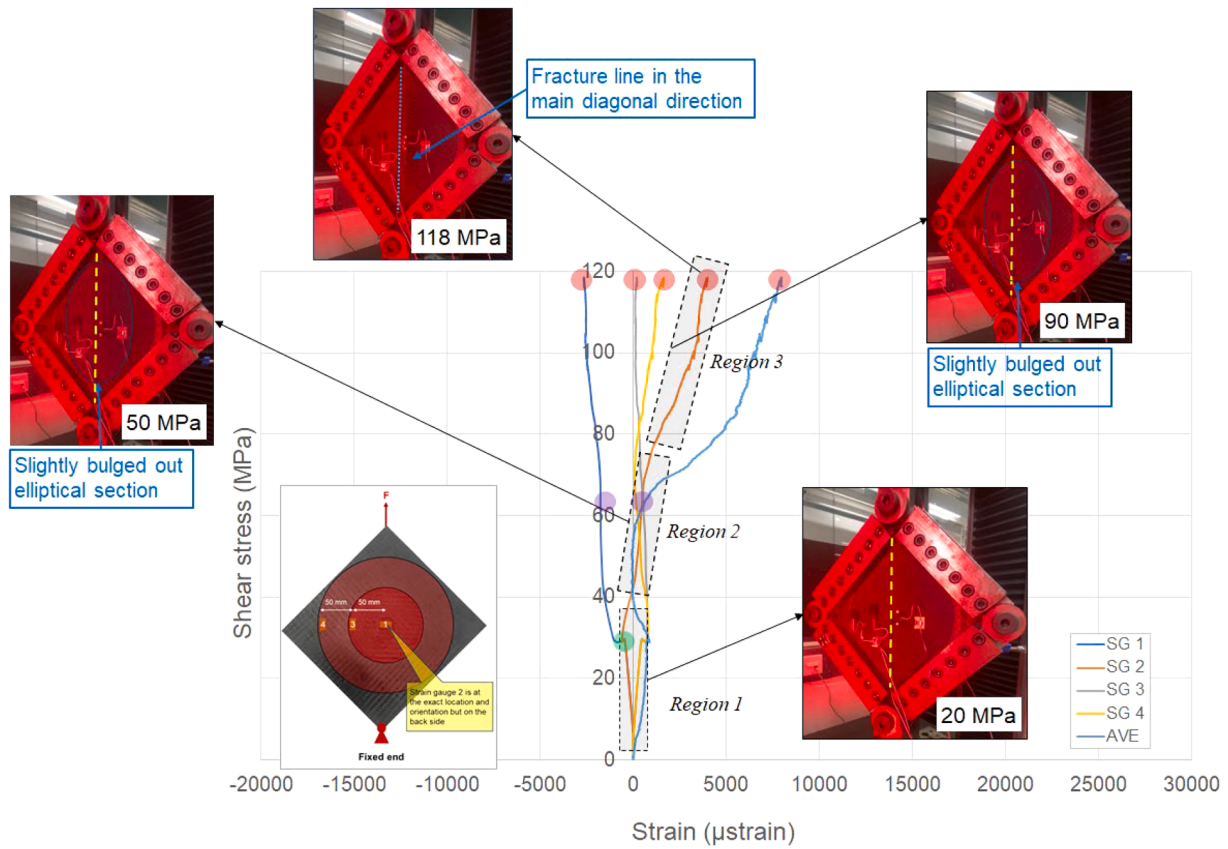

Fig. 17. Shear stress vs. strain of RS laminates.

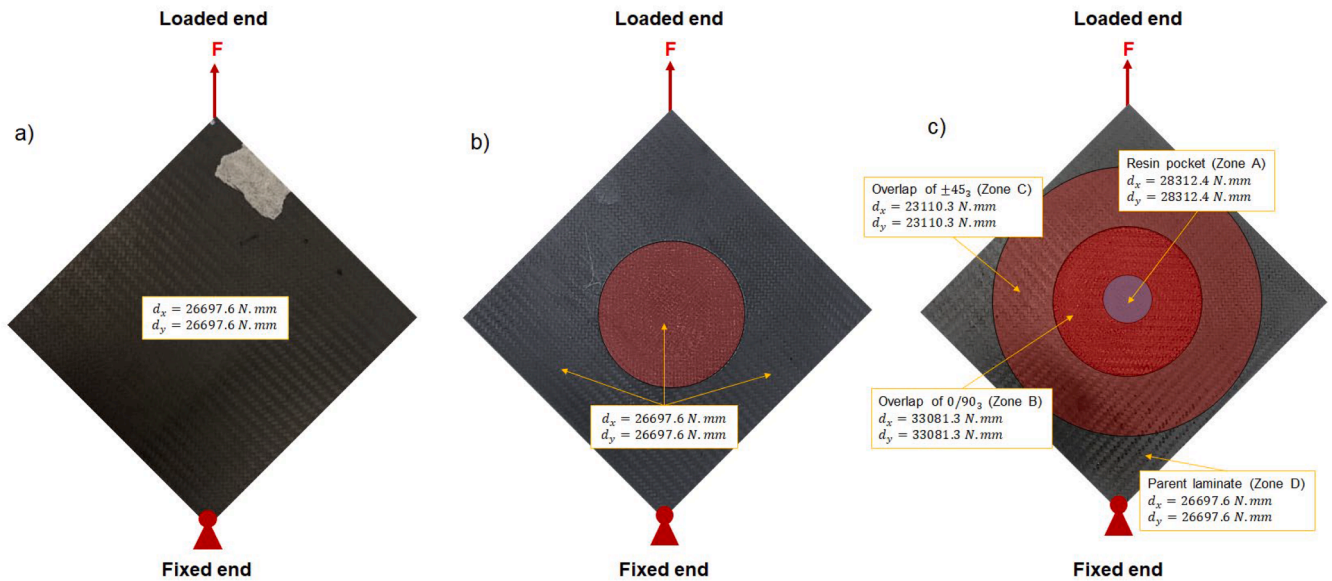**Fig. 18.** Shear stress vs. strain of SS laminates.
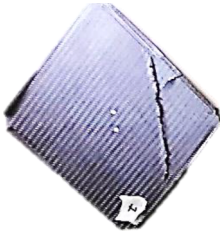
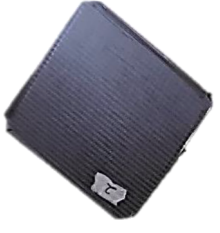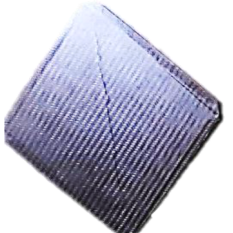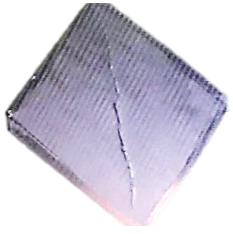**Fig. 19.** Illustration of bending stiffness of, a) Pristine, b) RS and c) SS laminates.

i.e. the top face. This failure mode aligns with the patterns reported in earlier work by the authors [32]. An exception to this pattern is specimen P1, which exhibited a failure path offset from the main diagonal, closer to the clamped boundary conditions. It is also noteworthy that specimens P2 and P3 did not exhibit any signs of fibre fracture on the tensile top surface. Instead, they showed fracture on the compressive bottom surface, suggesting a variation in the failure mechanism where compressive stresses on the bottom surface were sufficient to initiate

fracture before any tensile failure could occur on the top surface.

Based on Table 5, RS laminates exhibit a failure mode similar to that of pristine laminates. This outcome is expected because RS repairs involve minimal deviations from the structural configuration of pristine laminates. As a result, they are anticipated to cause minimal disruption to the original load path, provided that cohesive failure of the bond-line and detachment of the repair patch do not occur. However, detachment of the repair patch was observed in two of the RS laminates (RS2 and

Table 4
Failure mode of pristine specimens.

Specimen ID	Symmetric Failure	Repair Detachment	Pictures	
			Top surface	Bottom surface
P1	No	N/A		
P2 *	Yes	N/A		
P3 *	Yes	N/A		
P4	Yes	N/A		

* No damage is observed on the top surface.

RS4), suggesting that RS laminates may be more susceptible to repair patch detachment compared to SS laminates. This observation aligns with the findings of the authors' previous work [18], which indicated that RS repairs are more susceptible to stress concentrations due to the nature of their implementation. For further details on this aspect, the reader is referred to [18]. Despite the detachment, the failure mode and path of the RS laminates post-detachment remained consistent with those observed in pristine laminates.

According to Table 6, SS laminates also exhibit a similar failure mode to pristine ones. Only one SS specimen (SS4) showed repair patch detachment. As mentioned previously, this suggests that SS laminates are less prone to repair detachment compared to RS laminates. Nevertheless, after the repair patch detachment, the failure mode and path remain consistent with those of pristine laminates.

5. Conclusions

This study provides a comprehensive experimental investigation into the buckling and post-buckling behaviour of pristine (P) and repaired composite laminates under in-plane shear loading, using Ramped Scarf (RS) and Stepped Scarf (SS) repair techniques.

The findings from this study provide valuable insights into the buckling and post-buckling behaviour of composite laminates with different repair techniques under in-plane shear loading. The superior performance of RS repairs suggests that this technique may offer a more effective solution for restoring structural integrity, particularly in applications where post-buckling behaviour is critical. The results also highlight the importance of considering repair-induced stress concentrations and variability in performance, particularly for SS repairs.

The key findings of current study and their significance are outlined below:

Performance of RS Repairs:

○ RS repairs demonstrated superior mechanical performance compared to pristine laminates, with an average of 35 % higher maximum displacement and 12 % higher failure load. This indicates that RS repairs can effectively restore the load-bearing capacity of damaged laminates, making them a viable option for structural repair in aero-structural applications.
○ RS repairs outperformed SS repairs across all key mechanical performance indicators, including buckling load, Hooke's stiffness, maximum displacement, and failure load. This suggests that RS repairs are more effective in maintaining the structural integrity of repaired laminates under in-plane shear loading conditions.

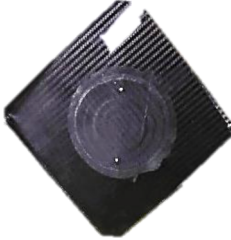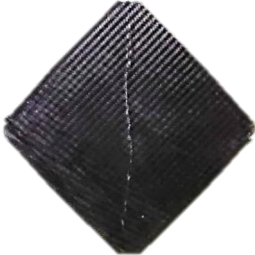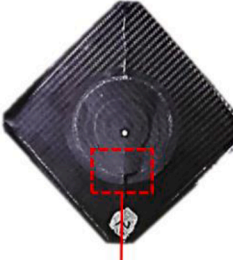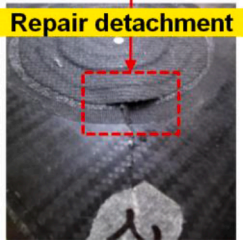**Table 5**
Failure mode of RS specimens.
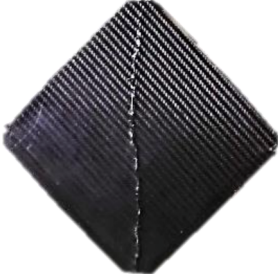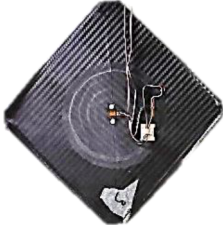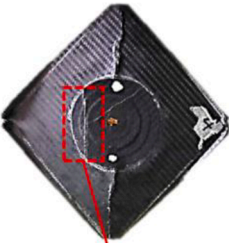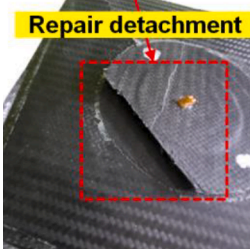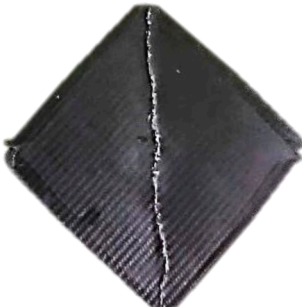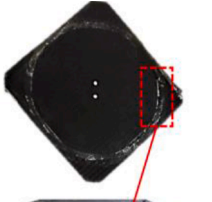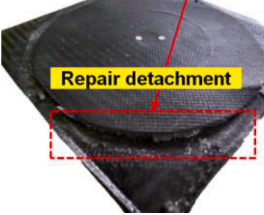
Specimen ID	Symmetric Failure	Repair Detachment	Pictures	
			Top surface	Bottom surface
RS1	Yes	No		
RS2	Yes	Yes	**Repair detachment**	
RS3	Yes	No		
RS4	No	Yes	**Repair detachment**	

Table 6

Failure mode of SS specimens.

Specimen ID	Symmetric Failure	Repair Detachment	Pictures	
			Top surface	Bottom surface
SS1	Yes	No		
SS2	Yes	No		
SS3	Yes	No		
SS4	No	Yes		

Performance of SS Repairs:

○ SS repairs showed a 19 % higher maximum displacement, and a 5 % higher failure load compared to pristine laminates, indicating a modest improvement in load-bearing capacity. However, SS repairs exhibited a more complex distribution of bending stiffness within the laminate, resulting in a stiffer stress-strain response.

○ The variability in bending stiffness within SS repairs, due to the offset between parent and overlapping repair plies, suggests that while SS repairs can enhance stiffness, they may also introduce stress concentrations that affect overall performance.

Stress-Strain Behaviour:

○ The stress-strain behaviour of both pristine and repaired laminates was generally similar. However, SS repairs demonstrated a more complex distribution of bending stiffness, leading to a stiffer response. This suggests that SS repairs, while maintaining the overall structural performance, may exhibit different mechanical characteristics due to their unique repair configuration.

Failure Modes and Repair Detachment:

○ The failure modes of P, RS, and SS laminates were generally similar, with fibre breakage being the primary mechanism. However, RS repairs exhibited a higher susceptibility to repair patch detachment compared to SS repairs, as observed in two RS specimens (RS2 and RS4). This aligns with previous findings indicating that RS repairs are more prone to stress concentrations due to their specific implementation.

○ Despite the detachment observed in RS repairs, the failure mode and path post-detachment remained consistent with those of pristine

laminates, suggesting that the repair still retains some structural capacity even after detachment.

Impact of Repair Techniques on Shear Buckling and Post-Buckling Behaviour:

○ Both RS and SS repairs provided similar performance in terms of shear buckling behaviour when post-buckling reserve is not a primary concern. However, RS repairs exhibited lower variability in key performance indicators, suggesting more consistent performance under similar loading conditions.
○ SS repairs, while less prone to detachment, showed higher variability in mechanical performance, likely due to the complex stress distribution introduced by the stepped configuration.

Design Considerations:

○ In structures where post-buckling reserve is a crucial consideration, RS repairs are preferred over SS repairs under in-plane shear loading. The superior performance of RS repairs in maintaining load-bearing capacity after buckling makes them suitable for applications where stability beyond the initial buckling event is important.
○ If only buckling resistance is critical and post-buckling reserve is not considered beneficial, both RS and SS repairs offer similar performance. However, RS repairs exhibited lower standard deviations in key mechanical performance indicators compared to SS repairs, indicating more consistent performance. Despite this, repair detachment after the buckling load was more predominant in RS repairs, which should be taken into account in design considerations.

6. Future research directions

Future work should focus on the following areas to further enhance the understanding and application of composite laminate repairs:

○ Investigating the buckling and post-buckling behaviour of RS and SS repaired stiffened panels under in-plane shear loading to assess the performance of these repair techniques in more complex structural configurations.
○ Examining the behaviour of both composite panels and stiffened composite panels under different loading conditions, such as uniaxial compressive and tensile loading, to provide a more comprehensive understanding of their performance.
○ Conducting detailed, fully nonlinear finite element analyses, similar to those described in references [30,32,42], is essential for a comprehensive understanding of the underlying mechanisms in the test scenarios. These analyses will provide further validation of the experimental findings, offering deeper insights into the structural behaviour and failure mechanisms that are difficult to capture through experimental methods alone.

These future studies will help to optimize repair techniques for various structural applications and improve the overall reliability and safety of composite structures.

CRediT authorship contribution statement

M. Damghani: Writing – review & editing, Writing – original draft, Visualization, Validation, Supervision, Software, Resources, Project administration, Methodology, Investigation, Funding acquisition, Formal analysis, Data curation, Conceptualization. **A. Bugaje:** Investigation, Data curation. **G.A. Atkinson:** Investigation, Data curation. **D. Cole:** Investigation, Data curation.

Declaration of competing interest

The authors declare that they have no known competing financial interests or personal relationships that could have appeared to influence the work reported in this paper.

Data availability

Data will be made available on request.

References

[1] M. Damghani, J. Matthews, A. Murphy, C. Featherston, Numerical shape, thickness and stacking sequence optimisation and experimental study of hybrid composite plates under in-plane shear loading, Structures 51 (2023) 372–390, https://doi.org/10.1016/j.istruc.2023.03.066.
[2] M. Suresh Kumar, M. Ambresha, K. Panbarasu, I. Kishore, V.R. Ranganath, A comparative study of failure features in aerospace grade unidirectional and bidirectional woven CFRP composite laminates under four-point bend fatigue loads, Materwiss Werksttech 46 (6) (2015) 644–651, https://doi.org/10.1002/mawe.201400278.
[3] G.-L. Song, C. Zhang, X. Chen, D. Zheng, Galvanic activity of carbon fiber reinforced polymers and electrochemical behavior of carbon fiber, Corrosion Communicat. 1 (2021) 26–39, https://doi.org/10.1016/j.corcom.2021.05.003.
[4] M. Damghani, et al., An experimental investigation of tensile residual strength of repaired composite laminates after low velocity impact, Thin Walled Struct. 200 (2024) 111896, https://doi.org/10.1016/j.tws.2024.111896.
[5] X. Li, Y. Gong, L. Jiang, Y. Zhao, N. Hu, A parametric study on the failure strength of multi-bolt composite repairs with different configurations, Theor. Appl. Fract. Mech. 121 (2022) 103459, https://doi.org/10.1016/j.tafmec.2022.103459.
[6] M. Ridha, V.B.C. Tan, T.E. Tay, Traction–separation laws for progressive failure of bonded scarf repair of composite panel, Compos. Struct. 93 (4) (2011) 1239–1245, https://doi.org/10.1016/j.compstruct.2010.10.015.
[7] C.H. Wang, C.N. Duong, Bonded Joints and Repairs to Composite Airframe Structures, Elsevier, 2016, https://doi.org/10.1016/C2013-0-00565-8.
[8] S. Budhe, M.D. Banea, S. de Barros, Bonded repair of composite structures in aerospace application: a review on environmental issues, Appl. Adhesion Sci. 6 (1) (2018) 3, https://doi.org/10.1186/s40563-018-0104-5.
[9] K.B. Katnam, L.F.M. Da Silva, T.M. Young, Bonded repair of composite aircraft structures: a review of scientific challenges and opportunities, Prog. Aerosp. Sci. 61 (2013) 26–42, https://doi.org/10.1016/j.paerosci.2013.03.003.
[10] J.-B. Orsatelli, E. Paroissien, F. Lachaud, E. Schwartz, Bonded flush repairs for aerospace composite structures: a review on modelling strategies and application to repairs optimization, reliability and durability, Compos. Struct. 304 (2023) 116338, https://doi.org/10.1016/j.compstruct.2022.116338.
[11] K.B. Katnam, L.F.M. Da Silva, and T.M. Young, "Bonded repair of composite aircraft structures: a review of scientific challenges and opportunities," 2013. doi:10.1016/j.paerosci.2013.03.003.
[12] B. Liu, F. Xu, W. Feng, R. Yan, W. Xie, Experiment and design methods of composite scarf repair for primary-load bearing structures, Compos Part A Appl. Sci. Manuf. 88 (2016) 27–38, https://doi.org/10.1016/j.compositesa.2016.05.011.
[13] B. Liu, F. Xu, R. Yan, Z. Ji, W. Li, Parameters sensitivity and optimization for composite scarf repair, J. Reinf. Plast. Compos. 33 (23) (2014) 2164–2173, https://doi.org/10.1177/0731684414555744.
[14] T.D. Breitzman, E.V. Iarve, B.M. Cook, G.A. Schoeppner, R.P. Lipton, Optimization of a composite scarf repair patch under tensile loading, Compos. Part A Appl. Sci. Manuf. 40 (12) (2009) 1921–1930, https://doi.org/10.1016/j.compositesa.2009.04.033.
[15] S. Psarras, T. Loutas, G. Galanopoulos, G. Karamadoukis, G. Sotiriadis, V. Kostopoulos, Evaluating experimentally and numerically different scarf-repair methodologies of composite structures, Int. J. Adhes. Adhes. 97 (2020) 102495, https://doi.org/10.1016/j.ijadhadh.2019.102495.
[16] S. Psarras, T. Loutas, M. Papanaoum, O.K. Triantopoulos, V. Kostopoulos, Investigating the effect of stepped scarf repair ratio in repaired CFRP laminates under compressive loading, J. Compos. Sci. 4 (4) (2020), https://doi.org/10.3390/jcs4040153.
[17] B. Liu, et al., Progressive damage behaviors of the stepped-lap composite joints under bending load, J. Compos. Mater. 54 (14) (2019) 1875–1887, https://doi.org/10.1177/0021998319889119. Nov.
[18] M. Damghani, et al., Design, novel quality check and experimental test of an original variable length stepped scarf repair scheme, Compos. B Eng. 230 (Feb. 2022) 109542, https://doi.org/10.1016/J.COMPOSITESB.2021.109542.
[19] J.-S. Yoo, V.-H. Truong, M.-Y. Park, J.-H. Choi, J.-H. Kweon, Parametric study on static and fatigue strength recovery of scarf-patch-repaired composite laminates, Compos. Struct. 140 (2016) 417–432, https://doi.org/10.1016/j.compstruct.2015.12.041.
[20] M. Niedernhuber, J. Holtmannspötter, I. Ehrlich, Fiber-oriented repair geometries for composite materials, Compos. B Eng. 94 (2016) 327–337, https://doi.org/10.1016/j.compositesb.2016.03.027.
[21] C.-H.K.M.-Y.P.J.-H.C. Viet-Hoai Truong Jae-Seung Yoo, J.-H. Kweon, Failure load prediction of laminates repaired with a scarf-bonded patch using the damage zone

method, Adv. Compos. Mater. 26 (2) (2017) 115–133, https://doi.org/10.1080/09243046.2016.1232008.

[22] E. Ghazali, M.-L.L. Dano, A. Gakwaya, C.-O.O. Amyot, Experimental and numerical studies of stepped-scarf circular repairs in composite sandwich panels, Int. J. Adhes. Adhes. 82 (2018) 41–49, https://doi.org/10.1016/j.ijadhadh.2017.12.008.

[23] E. Ghazali, M.-L.L. Dano, A. Gakwaya, C.-O.O. Amyot, Mechanical performance of repaired sandwich panels: experimental characterization and finite-element modelling, J. Sandwich Struct. Mater. 21 (4) (2019) 1357–1378, https://doi.org/10.1177/1099636217716059.

[24] L. Sun, Y. Tie, Y. Hou, X. Lu, C. Li, Prediction of failure behavior of adhesively bonded CFRP scarf joints using a cohesive zone model, Eng. Fract. Mech. 228 (2020) 106897, https://doi.org/10.1016/j.engfracmech.2020.106897.

[25] R.D.S.G. Campilho, M.F.S.F. de Moura, D.A. Ramantani, J.J.L. Morais, J.J.M. S. Domingues, Buckling behaviour of carbon–epoxy adhesively-bonded scarf repairs, J. Adhes. Sci. Technol. 23 (10–11) (2009) 1493–1513, https://doi.org/10.1163/156856109×433045.

[26] R.D.S.G. Campilho, M.F.S.F. de Moura, D.A. Ramantani, J.J.L. Morais, J.J.M. S. Domingues, Buckling strength of adhesively-bonded single and double-strap repairs on carbon-epoxy structures, Compos. Sci. Technol. 70 (2) (2010) 371–379, https://doi.org/10.1016/j.compscitech.2009.11.010.

[27] K. Turan, Buckling behavior of adhesively patch-repaired composite plates, J. Compos. Mater. 48 (26) (2013) 3253–3261, https://doi.org/10.1177/0021998313508801.

[28] J. Deng, G. Zhou, S.P.A. Bordas, C. Xiang, D. Cai, Numerical evaluation of buckling behaviour induced by compression on patch-repaired composites, Compos. Struct. 168 (2017) 582–596, https://doi.org/10.1016/j.compstruct.2016.12.071.

[29] A. Ghiamy, H. Amoushahi, Dynamic stability of different kinds of sandwich plates using third order shear deformation theory, Thin Walled Struct. 172 (2022) 108822, https://doi.org/10.1016/j.tws.2021.108822.

[30] H. Tanzadeh, H. Amoushahi, Analysis of laminated composite plates based on different shear deformation plate theories, Struct. Eng. Mech. 75 (2) (Jul. 2020) 247–269.

[31] G. Viana, M. Costa, M.D. Banea, L.F.M. da Silva, A review on the temperature and moisture degradation of adhesive joints, Proc. Inst. Mech. Eng. Part L J. Mater. Des. Appl. 231 (5) (2017) 488–501, https://doi.org/10.1177/1464420716671503.

[32] M. Damghani, C. Wallis, J. Bakunowicz, A. Murphy, Using laminate hybridisation (CFRP-GFRP) and shaped CFRP plies to increase plate post-buckling strain to failure under shear loading, Thin Walled Struct. 162 (2021) 107543, https://doi.org/10.1016/j.tws.2021.107543.

[33] M. Damghani, J. Saddler, E. Sammon, G.A. Atkinson, J. Matthews, A. Murphy, An experimental investigation of the impact response and Post-impact shear buckling behaviour of hybrid composite laminates, Compos. Struct. 305 (2023) 116506, https://doi.org/10.1016/j.compstruct.2022.116506.

[34] M. Damghani, R.A. Pir, A. Murphy, M. Fotouhi, Experimental and numerical study of hybrid (CFRP-GFRP) composite laminates containing circular cut-outs under shear loading, Thin Walled Struct. 179 (2022) 109752, https://doi.org/10.1016/j.tws.2022.109752.

[35] J.Y. Goh, S. Georgiadis, A.C. Orifici, C.H. Wang, Effects of bondline flaws on the damage tolerance of composite scarf joints, Compos Part A Appl Sci Manuf 55 (2013) 110–119, https://doi.org/10.1016/j.compositesa.2013.07.017.

[36] M.K. Kim, D.J. Elder, C.H. Wang, S. Feih, Interaction of laminate damage and adhesive disbonding in composite scarf joints subjected to combined in-plane loading and impact, Compos. Struct. 94 (3) (2012) 945–953, https://doi.org/10.1016/j.compstruct.2011.10.017.

[37] U.A. Khashaba, I.M.R. Najjar, Adhesive layer analysis for scarf bonded joint in CFRE composites modified with MWCNTs under tensile and fatigue loads, Compos. Struct. 184 (2018) 411–427, https://doi.org/10.1016/J.COMPSTRUCT.2017.09.095.

[38] J.Y. Cognard, L. Sohier, P. Davies, A modified Arcan test to analyze the behavior of composites and their assemblies under out-of-plane loadings, Compos. Part A Appl. Sci. Manuf. 42 (1) (2011) 111–121, https://doi.org/10.1016/J.COMPOSITESA.2010.10.012.

[39] M. Damghani, J. Saddler, E. Sammon, G.A. Atkinson, J. Matthews, A. Murphy, An experimental investigation of the impact response and Post-impact shear buckling behaviour of hybrid composite laminates, Compos. Struct. 305 (2023) 116506, https://doi.org/10.1016/j.compstruct.2022.116506.

[40] S. Budhe, M.D. Banea, S. de Barros, L.F.M. da Silva, An updated review of adhesively bonded joints in composite materials, Int. J. Adhes. Adhes. 72 (2017) 30–42, https://doi.org/10.1016/j.ijadhadh.2016.10.010.

[41] M. Damghani, M. Saad Khan, G.A. Atkinson, Experimental study of bonded, bolted, and hybrid bonded-bolted single lap shear joints with woven CFRP adherends, Compos. Struct. 334 (2024) 117989, https://doi.org/10.1016/j.compstruct.2024.117989.

[42] P. Rozylo, H. Debski, Stability and load-carrying capacity of short composite Z-profiles under eccentric compression, Thin Walled Struct. 157 (2020) 107019, https://doi.org/10.1016/j.tws.2020.107019.